55. Copper and Silver Atoms in the β-Cage of a Zeolite: Model Calculations

by **Gion Calzaferri*** and **Lars Forss**

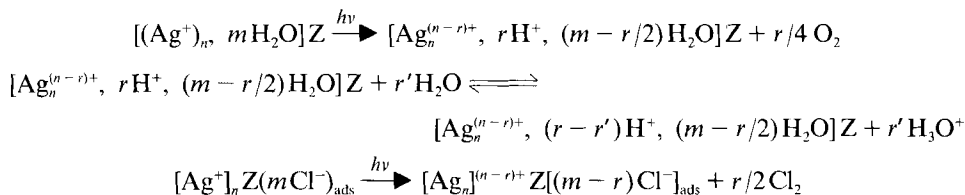Institute for Inorganic and Physical Chemistry, University of Bern, CH–3000 Bern 9

(20.XI.86)

The electronic structures of the 4-4 SBU, the 6-6 SBU, the β-cage, and the β-cage with two 4-4 SBU's attached to it have been studied by means of EH-MO calculations. No indication of the formation of a band structure has been found. The HOMO region consists of many closely spaced, localized states, 98.6% of them concentrated on the O-atoms. Reversible color changes of Cu^{+1} and Ag^{+1} zeolites observed upon hydration-dehydration experiments can be understood as charge-transfer transitions from the HOMO concentrated on the zeolite O-atoms to the metal cations. As soon as the Cu^{+1} or Ag^{+1} are partially hydrated, the ns* and np* states are shifted to higher energies. The luminescence observed with dehydrated Cu^{+1}-zeolites X is caused by a 4p*←HOMO absorption, followed by spontaneous 4s*←4p* emission. After a detailed study of a Cu^{+1} in the 6-6 SBU, we discuss the electronic structure of a β-cage filled with 1, 2, 4, 8, and 9 Cu^{+1}. In each case, the β-cage is found to be too small to allow the formation of a band structure. The levels caused by the added copper are distinctly quantized. Calculations on $[Ag_3(H_2O)_3]^{3+}$ in a β-cage are reported. The direct interaction between the Ag-atoms is significant. As a consequence, the states formed by Ag 5s and 5p atomic orbitals are delocalized over the three Ag-centers. In both the Cu^{+1} and the Ag^{+1} zeolites, the ligand-field picture is found to be insufficient to explain the electronic structure, when the metal is coordinated to the zeolite oxygen framework.

1. Introduction. – In previous model calculations, we have studied the electronic structures of a 4-4 SBU (secondary building unit) (D4R) and of 6-6 SBU (D6R) of a zeolite, and their changes after the addition of Cu- or Ag-atoms [1] [2]. We now apply the experience gained in these studies to the β-cage. Because of its loose structure, the β-cage opens many more degrees of freedom regarding interactions with molecules, ions, or atoms, and consequently the complexity increases [3]. First, we describe how the electronic structure develops from the 4-4 SBU to the 6-6 SBU, to the β-cage, and to the β-cage with two 4-4 SBU's attached to it. We then study the alteration of the electronic structure upon adding Cu- and Ag-atoms and compare the behavior of the two metal species. Because of the many degrees of freedom, many different situations have to be investigated, and the question arises, whether statistical models should be applied. Here, we prefer to study some specific cases and to connect them by means of correlation diagrams. Several quantum-chemical studies on different properties of zeolites [4] and of zeolites containing metal cations or reduced metal centers [5] have been published. No MO calculations on the whole β-cage and on the β-cage interacting with Cu or Ag species have appeared up to now. Hydrogen uptake of Cu or Ag-Y-zeolites and reoxidation with O_2 has been studied by *Riekert*. The behavior of the Ag-Y zeolite towards H_2 and O_2 was found to be consistent with the assumption that reduced Ag particles are reoxidized to Ag^+ ions in the lattice, and that no Ag_2O was formed [6]. The consumption of hydrogen over Ag^+-Y and of oxygen over Ag^0-Y zeolites was followed kinetically. IR and X-ray spectroscopy [7] and later also ESR measurements [8] were used to characterize the reactions. It was suggested in 1962 that the reversible color changes observed upon

dehydration-hydration in Ag-A zeolites could be used for visible inspection of small amounts of H_2O [9]. Optical spectra of Ag-exchanged zeolites and color centers created upon dehydration have been reported by several authors [7–15]. These color changes were attributed to an autoreductive process involving framework oxygen and formation of Ag^0 [13] [14]. In very recent EPR and magnetic susceptibility measurements of Ag-Y zeolites, however, the presence of Ag^0 in dehydration experiments could not be confirmed, and doubts were expressed about previous assignments of optical bands to Ag^0-atoms. Ag^0 could only be observed after γ-irradiation, and the radiolytically produced Ag^0 centers were found to be unstable at temperatures above 77 K [16–20].

Part of our interest in the electronic structure of Ag zeolites is due to their redox and photoredox properties [6] [7] [21–26]. With Ag zeolites in aqueous dispersions, we have detected self-sensitization in the visible spectrum of the photochemical production of O_2 and Cl_2 from H_2O and Cl^-, respectively [23–26]. By self-sensitization, we mean that dispersions which are initially insensitive to light of a certain wavelength become photo-active, after they have been illuminated by light of higher energy. According to our present knowledge, the overall stoichiometry of this photo-oxygen and photochlorine generation can be described as follows:

$$[(Ag^+)_n,\ mH_2O]Z \xrightarrow{h\nu} [Ag_n^{(n-r)+},\ rH^+,\ (m-r/2)H_2O]Z + r/4\ O_2$$

$$[Ag_n^{(n-r)+},\ rH^+,\ (m-r/2)H_2O]Z + r'H_2O \rightleftharpoons$$

$$[Ag_n^{(n-r)+},\ (r-r')H^+,\ (m-r/2)H_2O]Z + r'H_3O^+$$

$$[Ag^+]_n Z(mCl^-)_{ads} \xrightarrow{h\nu} [Ag_n]^{(n-r)+} Z[(m-r)Cl^-]_{ads} + r/2\ Cl_2$$

Z = zeolite framework

When metal cations are reduced on a zeolite support in a photoredox reaction, very finely dispersed metal atoms and metal clusters are produced. We are interested to know more about the reactivity of the photochemically produced Ag clusters.

The green luminescence of Cu(I) zeolites described by *Maxwell* and *Drent* [27] was further studied by *Texter et al.* [28] and found to be useful to establish the reduction conditions in an H_2 or in a CO atmosphere for a complete conversion of $Cu^{+II}Y$ zeolites to $Cu^{+I}Y$, but not further to Cu^0Y [29–31]. The Cu^{+I} ions in type-Y zeolites were reported to be specific adsorption centers for CO [30] and ethylene [32], and to catalyze the oxydation of CO [33] [34]. Excitation of the Cl^- to copper-charge-transfer states of an aqueous acidic CuCl solution with light of shorter wavelength than 330 nm causes photochemical H_2 production and oxidation of the Cu^{+I} to Cu^{+II} [35] [36].

2. Electronic Structure of the β-Cage. – In this chapter, we describe the development of the electronic structure from the 4-4 SBU to the 6-6 SBU, to the β-cage, to the β-cage with two 4-4 SBU's attached to it, and we discuss the influence of charge-compensating cations. Although X-ray [37] [38] and theoretical [4] studies have been published, it is not easy to know the exact positions of the charge-compensating alkali cations, because they can occupy several equivalent or nearly equivalent sites, and because the degree of dehydration plays an important role. The information needed for our purpose can be obtained by comparing the uncharged $(OH)_8Si_8O_{12}$ (I') with $[(OH)_8Si_4Al_4O_{12}]^{4-}$ (I), as shown in *Fig. 1*. It is reasonable to expect that the MO levels of $[(OH)_8Si_{4+n}Al_{4-n}O_{12}]^{(4-n)-}$,
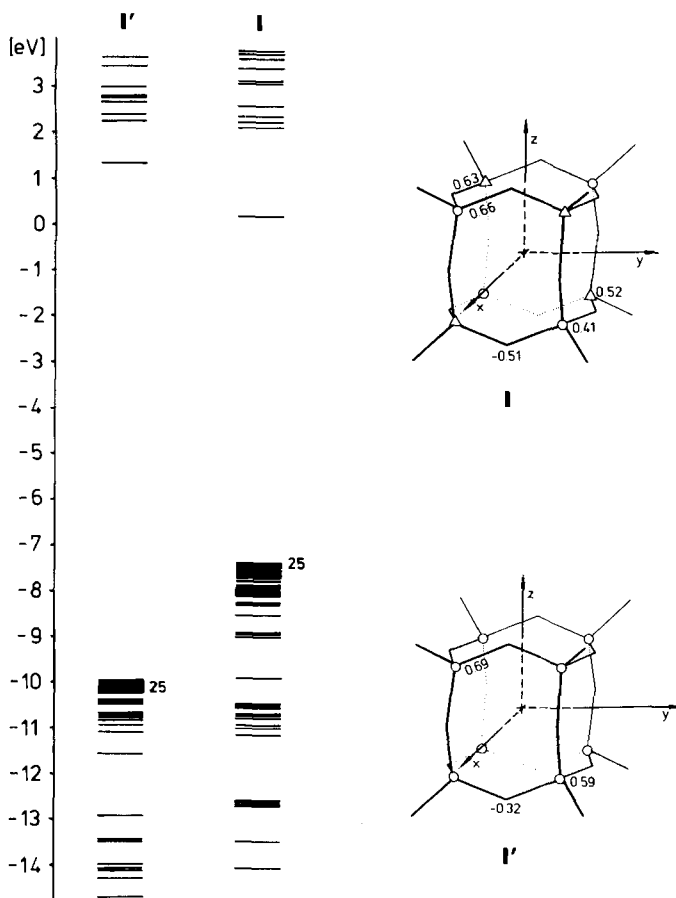
Fig. 1. *Comparison of the electronic structure, the charge distribution, and the overlap population of* [(HO)$_8$Si$_8$O$_{12}$] (I') *with* [(HO)$_8$Si$_4$Al$_4$O$_{12}$]$^{4-}$ (I). ○ = Si, △ = Al. Overlap populations are on the left half of the skeletons of I and I'.

(n = 0, 1, 2, 3, 4) species lie between the ones of I' and I and that the addition of charge-compensating alkali ions causes a shift of the levels in direction of I'. As in the case of the 6-6 SBU [2], the HOMO region consists of nonbonding localized orbitals on the O-atoms. The energy difference of the MO levels between I' and I is due to the different *Coulomb* parameters for Si and Al which are obtained in the charge-iteration procedure *(Table 1)*. The measured first-ionization potential of SiO (IP_1 = 11.43 eV [40], calculated 11.38 eV) and of AlO (IP_1 = 9.53 eV [40], calculated 10.53 eV) differ by 1.9 eV. With these observed and calculated ionization potentials of the diatomic molecules, the large energy difference between the HOMO of I and I' seems reasonable. In this context, we would like to mention that the synthesis of X$_8$[Si$_8$O$_{12}$] (X = H, Cl, CH$_3$O) has been published [39] [41] and reproduced in our laboratory. The study of these molecules will improve the connection between theoretical and experimental results.

All calculations reported here have been carried out by means of the EH-MO method [42] with charge iteration [43]. The weighted *Wolfsberg-Helmholz* formula [44] with

Table 1. *Parameters Used in the EH-MO Calculations*

	H	O		Al		Si		Cu			Ag		
	1s	2s	2p	3s	3p	3s	3p	4s	4p	3d	5s	5p	4d
A) Atomic -H_{ii} parameters in [eV]													
H_2O	16.38	27.99	12.3										
AlO		26.87	11.4	14.1	8.22								
SiO		26.98	11.49			17.93	10.30						
I′		25.26	10.12			11.72	14.31						
I		22.0	7.5	16.77	10.38	20.26	12.26						
Cu^{+1}-**I′**								10.98	5.80	13.93			
Cu^{+1}-**I**								8.83	4.31	12.08			
Cu^{+1}-6-6 SBU (0,0,0)								7.88	3.79	10.89			
Cu^{+1}-6-6 SBU (0,0,2)								8.42	4.08	11.51			
$(Cu^{+1})_n$-β								8.83	4.31	12.08			
Ag^{+1}-6-6 SBU (0,0,0)											9.77	8.54	14.30
$[Ag_3(H_2O)_3]^{3+}$-s H_2O	16.38	27.99	12.3								9.77	8.54	14.30
β		21.99	7.5								9.77	8.54	14.30
B) Slaterexponents													
	1.3	2.275	2.275	1.167	1.167	1.38	1.38	1.85	1.55	5.95 (0.599)	1.54	0.92	6.07 (0.559)
										2.3 (0.568)			2.66 (0.605)

$k = 1.75$ has been applied to approximate the off-diagonal elements. Charge-iteration parameters have been taken from [45] and for Ag from [46]. *Mulliken* population analysis has been applied [47]. As in [2], charge iteration on **I** and **I′** was carried out on all Si, Al centers, and on the O-atoms between them. We have always set the H_{ii} of the terminal O-atoms equal to the values of those belonging to the bridging O-atoms. All T–O (T = Si, Al) distances were chosen 1.63 Å. We found that using unequal Al–O, Si–O bond lengths does not change the results reported, whereas a fully symmetric structure makes the interpretation easier. Charge iteration on Ag and Cu has been carried out for a number of cases reported in *Table 1* where the parameters are listed.

In *Fig. 2*, we show the structure and the coordinate system of the cages discussed in this paper as well as the calculated charge distribution and bond order. Structural data have been taken from X-ray studies in [37]. If not otherwise indicated, the Si/Al ratio was chosen equal to 1 with strict alternation. This choice makes the interpretation of the calculations much easier for symmetry reasons.
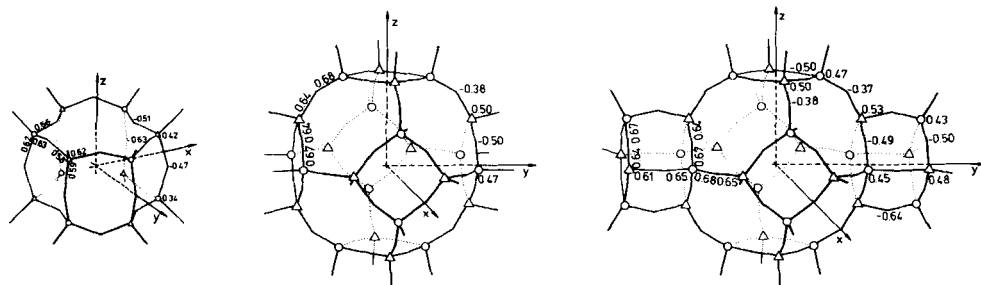

Fig. 2. *Structure, coordinate system, charge distribution, and overlap population* (from left to right) *of the 6-6 SBU, the β-cage, and the β-cage with two 4-4 SBU's attached to it.* ○ = Si, △ = Al. Overlap populations are on the left of the skeletons.

Considering the size of the β-cage, one might expect a band structure to develop. In *Fig. 3*, where we compare the one-electron levels of the 4-4 SBU, the 6-6 SBU, the β-cage, and the β-cage with two 4-4 SBU's attached to it, we do not find any indication that a conduction band is formed. The question arises, whether the occupied frontier orbitals, indicated as a black bar, can be interpreted as the beginning of a valence band of the many energetically narrow-lying O orbitals. To find an answer, we should look at these orbitals more closely. The reduced *Mulliken* charge distribution of the orbitals in the black bar is given in *Table 2*. The values indicate that in each case more than 98.6% of the electron density is localized on the p orbitals of the O-atoms. The number of one-electron levels in this region increases from 35 to 52 to 107 and to 163 with the number of O-atoms. In *Table 3*, we have collected the nearest neighbour Si–O, Al–O, O–O, and Al–Si overlap integrals. The 2p–2p overlap integrals between the adjacent O-atoms are very small. This

Table 2. *EH-MO Charge Distribution of the Orbitals in the Black Bar Region in %*

	4-4 SBU	6-6 SBU	β-cage
O	98.83	98.67	98.66
Si	0.29	0.34	0.34
Al	0.88	0.99	1.0

Table 3. *Overlap Integrals at Mean Bond Distance between the Indicated Atoms*

$O \xrightarrow{2.62} O \longrightarrow x$

O/O	s	p_x	p_y	p_z
s	0.0075	−0.0109	0.0	0.0
p_x	0.0109	−0.0157	0.0	0.0
p_y	0.0	0.0	0.0020	0.0
p_z	0.0	0.0	0.0	0.0020

$Al \xrightarrow{1.63} O \longrightarrow x$

O/Al	s	p_x	p_y	p_z
s	0.3179	−0.4702	0.0	0.0
p_x	0.1313	−0.1597	0.0	0.0
p_y	0.0	0.0	0.1608	0.0
p_z	0.0	0.0	0.0	0.1608

$Si \xrightarrow{1.63} O \longrightarrow x$

O/Si	s	p_x	p_y	p_z
s	0.3053	−0.4462	0.0	0.0
p_x	0.1729	0.2205	0.0	0.0
p_y	0.0	0.0	0.0962	0.0
p_z	0.0	0.0	0.0	0.0962

$Si \xrightarrow{3.20} Al \longrightarrow x$

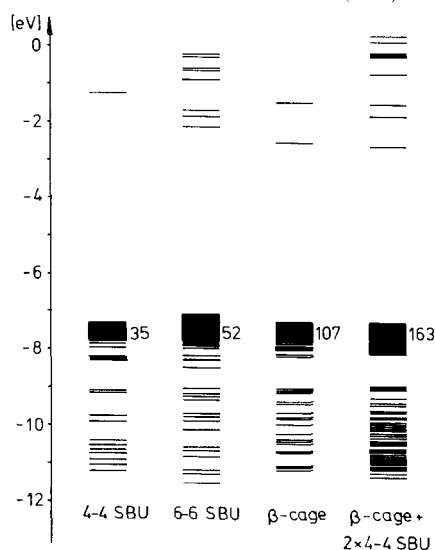| Al/Si	s	p_x	p_y	p_z
s	0.2032	−0.2293	0.0	0.0
p_x	0.2726	0.2928	0.0	0.0
p_y	0.0	0.0	0.0962	0.0
p_z	0.0	0.0	0.0	0.0962

Fig. 3. *Electronic structure of the 4-4 SBU, the 6-6 SBU, the β-cage, and the β-cage with two 4-4 SBU's attached to it*

means that the conditions for the development of a delocalized p-band structure are not fulfilled. Therefore, the black-bar region has to be interpreted as a region of energetically narrow-lying, localized states which only weakly interact with each other. Furthermore, there is no indication that a conduction band will develop in the region of the unoccupied orbitals. Inclusion of d orbitals does not have any significant influence on the highest-occupied orbitals. They help to get higher state densities in the LUMO region, but they do not lead to a situation which can be described as a conduction band, in the sense as this term is used today. For simplicity and in order to save computer time, we have not included d orbitals on Si- and Al-centers without losing much information.

3. Development of the Electronic Structure of a β-Cage upon Adding Cu-Atoms. – Prior to studying the β-cage, we examine the electronic structure of Cu^{+1} in the 4-4 SBU, in various sites of the 6-6 SBU and coordinated by two H_2O molecules in the 6-ring of the 6-6 SBU. Again, it is of interest how much the Al/Si ratio influences the electronic structure. Let us, therefore, compare Cu^{+1} in the center of cage **I** with Cu^{+1} in the center of cage **I′**, by carrying out charge iteration on the copper. The results in *Fig. 4* show that the HOMO-4s* and the HOMO-4p* energy difference remains the same in both cases. This means that the copper H_{ii} values follow the ligand levels almost perfectly. Because the interaction of Cu species with the ligand is almost completely determined by the oxygen, the levels are only shifted but not much changed in their character. This is a very important result, because it tells us that the pattern of the energy diagrams reported in this study are not much influenced by small changes of the position of the HOMO. If we replace the absolute energy scale by a relative scale in the following diagrams, there is good reason to expect them to be generally valid.

The correlation diagram in *Fig. 5* demonstrates that Cu^{+1} located at different positions of a zeolite framework should exhibit different behavior. For a Cu^{+1} in the 4-4 SBU, an oxygen-to-metal charge transfer is expected in the blue-yellow region, while in case of Cu^{+1} in the 6-6 SBU the same type of transition will occur in the deep red or near IR
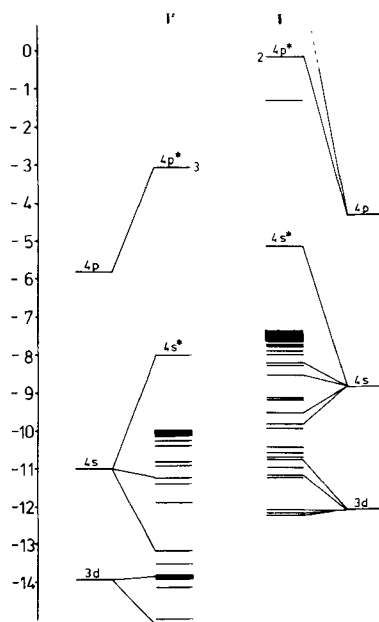
Fig. 4. *Comparison of the electronic structure of a* Cu^{+1} *in the 4-4 SBU* **I** *and* **I'**. The degeneracies of the 4s* and 4p* levels are 1 and 2, respectively, in case **I**, and 1 and 3 in case **I'**.

region, depending on the position of the Cu-atom. If Cu^{+1} is coordinated by two H_2O molecules, all electronic transitions are shifted into the UV region. Antibonding interaction with the 'water-oxygen' is the reason why the 4s* orbital is shifted to much higher energies. In this case, the situation of Cu^{+1} fully coordinated by H_2O is approached where electronic transitions occur only in the far UV. It is very interesting to recognize the difference between the Cu^{+1} coordinated by the 6-ring of the 6-6 SBU and two H_2O molecules and the Cu^{+1} coordinated by two H_2O molecules only. The orbital stabilization energy ΔE on the top of *Fig. 5* show that Cu^{+1} is more stable in the 4-4 SBU than in the 6-6 SBU, and that hydration of the Cu^{+1} coordinated by the 6-ring is an exothermic process. A simple crystal-field picture is obviously not adequate to describe the main patterns of the optical spectra of copper coordinated by a zeolite, but it is sufficient to describe many aspects of fully hydrated Cu ions. In each case shown in *Fig. 5*, a 4s*←3d transition is expected to occur in the UV. From the spectroscopic data reported by *Texter et al.* [28], we know that a hydrated Cu^{+1}-Y zeolite shows a broad absorption slowly starting at approximately 28 500 cm^{-1}. After dehydration, a second absorption band with a maximum at approximately 11 000 cm^{-1} is observed. If a dehydrated zeolite is irradiated in the UV, luminescence with an emission maximum of approximately 18 000 cm^{-1} occurs. According to the MO diagram in *Fig. 5*, this emission is due to a 4s*←4p* transition, and the UV absorption is mainly due to a 4p*←HOMO charge-transfer transition. Because the 3d levels are below the HOMO region, we expect that 4s*←3d transitions can not cause significant luminescence. Internal conversion due to strong coupling with lattice vibrations is expected to be very fast in this case. Because of the high state density in the HOMO region and the charge-transfer nature of the HOMO(1)4s*(2) configuration, we expect the exchange integral

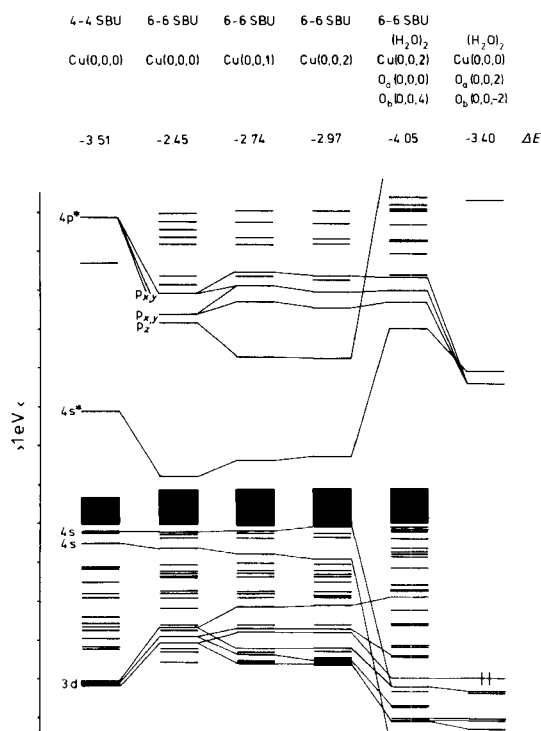Fig. 5. *Correlation diagram of the Cu^{+1} in the 4-4 SBU, in the 6-6 SBU, and hydrated Cu^{+1} in the 6-6 SBU as well as a Cu^{+1} coordinated by 2 H$_2$O molecules only.* The positions of the Cu^{+1} and the H$_2$O are indicated as (x,y,z) coordinates in [Å]. ΔE is the orbital stabilization energy in [eV].

$$\langle HOMO(1)\,4s^*(2)\,|\,1/r_{12}\,|\,HOMO(2)\,4s^*(1)\rangle$$

of an electron in the HOMO and one in the 4s* orbital to be small, and as a result the singlet-triplet splitting should not be large; HOMO represents the whole black-bar region.

The Cu^{+1} radius is 0.96 Å, the radius of the hole of the 6-6 SBU is in the order of 1.56 Å, and the hexagonal hole of the 6-ring has a radius of about 1.25 Å. To get an idea about the equilibrium position of the Cu^{+1} and the shape of the potential-energy curve, we have calculated the relative stability ΔE

$$\Delta E = E(\text{ligands} + Cu^{+1}) - E(Cu^{+1}) - E(\text{ligands})$$

of the Cu^{+1} at different positions of the 6-6 SBU. At each point, charge-iteration on the metal was carried out. If charge iteration is applied, only the orbital stabilization energy ΔE_{orb} has a meaning. Therefore, the energy has to be calculated in terms of

$$\Delta E_{orb} = \Sigma_i\, n_i\, \varepsilon_i - \Sigma_\alpha\, n_\alpha\, h_{\alpha\alpha}$$

where the ε_i are the one-electron energies, n_i the occupation of the orbitals, $h_{\alpha\alpha}$ the *Coulomb* integrals after charge iteration and n_α the occupations of the corresponding atomic orbitals [48].
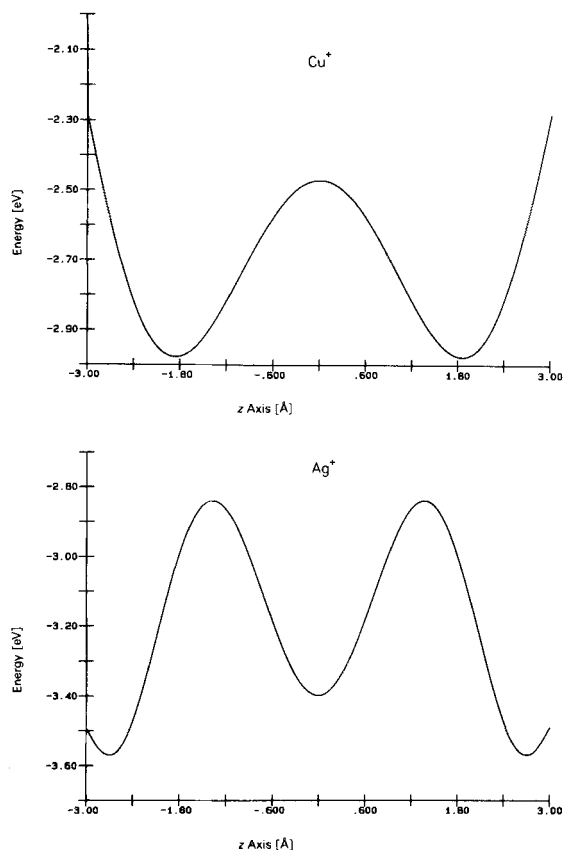
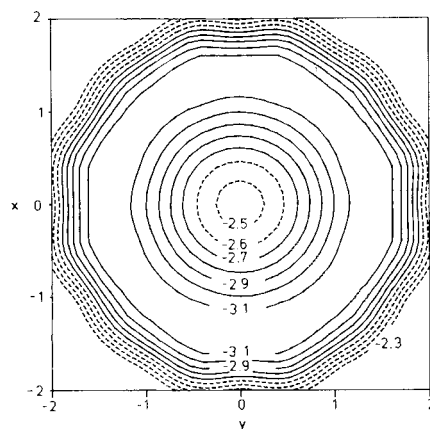Fig. 6. *Potential-energy curves of Cu⁺ and Ag⁺ in the 6-6 SBU along the z axis*

Fig. 7. *Contour diagram of the potential energy of* Cu^{+1} *in the 6-6 SBU in the* xy *plane at* $z = 0$. Energy in [eV] and distance in [Å].

The results of this calculation are shown in *Figs. 6* and *7*. For Cu^{+1}, we find a double minimum along the z axis that lies nearly in the center of the two 6-rings *(Fig. 6a)*, while in the xy plane, there is a flat minimum valley of circular symmetry *(Fig. 7)* that is about as deep as the minimum along the z axis. Combination of the two figures suggests an ellipsoidal equipotential surface and, therefore, an ellipsoidal residence probability of the Cu^{+1} in the 6-6 SBU. This is an unfamiliar way of describing the potential energy of a cation in a cage. Instead of a minimum position, we have to think in terms of a minimum shell of ellipsoidal aspect.

It follows from *Fig. 5* that the HOMO-4s* energy difference is larger on this ellipsoidal surface than in the center of the cage because of antibonding interactions similar to those discussed in an earlier paper (see Fig. 3 of [2]). Interestingly, upon excitation into the $(HOMO)^{n-1}(4s^*)^1$ charge-transfer state or upon reduction to Cu^0, the copper slips into the center of the cage.

The interpretation of the absorption and emission of a dehydrated zeolite as suggested by the MO calculations is summarized in *Fig. 8*. The absorption observed below 350 nm is caused by the 4p*←HOMO charge-transfer transition *2* and perhaps mixed to some
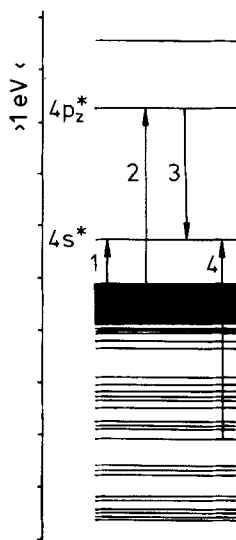
Fig. 8. *Interpretation of the absorption and emission of dehydrated Cu^{+I} zeolite Y*
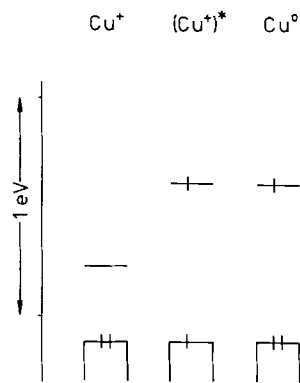
Fig. 9. *HOMO-4s* energy levels of Cu^0, Cu^{+I}, (Cu^{+I})* in the center of the 6-6 SBU*

extent with the 4s*←3d transition 4. The 4s*←HOMO charge-transfer transition 1 is responsible for the absorption in the near IR with a maximum at 11 000 cm^{-1}, and the 4s*←4p* transition 3 describes the green emission which is observed after UV excitation.

For Ag$^+$ in the 6-6 SBU, which has already been discussed in the paper mentioned above, we find a minimum in the center as well as one outside of the cage. The reason for this different behavior of Cu(I) and Ag(I) is the pronounced difference in size of the two isoelectronic metal cations.

Reduction of Cu^{+I} to Cu^0 means in this picture to put an electron into the 4s* level. The process of reduction induces not only a change of the coordination, but we would also expect the 4s* level to shift to higher energies. This shift of the 4s* level can easily be understood in terms of the EH-MO picture with charge iteration; similar processes are observed in many redox reactions and charge-transfer transitions [48]. If the charge density is increased on the metal either by reduction or by a charge-transfer transition, the metal tries to reduce this charge density by adapting the H_{ii} to the new situation. Cases in which crossing of metal-centered orbitals with ligand-centered ones can occur have been discussed recently [1]. In *Fig. 9*, we show the change of the 4s* orbital energy caused by occupation either in a redox process or in a charge-transfer transition.

If Cu^{+I} in the 6-6 SBU is oxidized, we expect the Cu^{+II} to move closer to 3 of the 6 O-atoms of the 6-ring, because its diameter is approximately 2.5 Å, while that of the Cu^{+II} is 1.44 Å only. In this new position, much stronger antibonding interaction of the Cu d-orbitals with the zeolite O orbitals occurs. The d-type orbitals shift to higher energies, but we do not expect them to cross the HOMO region of the nonbonding O-orbitals, unless the copper is partially solvated. Because of its small radius and the fast rate at which H$_2$O exchange occurs, Cu^{+II} is very mobile. It appears that Cu^{+II} in a wet zeolite can form complexes of nearly every symmetry during the various solvation and activation treatments reported in [49] [50]. In recent electron-spin-resonance studies of ZK4-Cu^{+II}, it

was possible to identify Cu^{+II} at octahedral, tetrahedral, and trigonal-bipyramidal coordination [51].

With this information, we now try to get a picture about what happens, if more than one Cu^{+I} occupies a β-cage. As long as the zeolite is fully hydrated and only one Cu^{+I} present, we expect a very similar MO picture to the hydrated copper in the 6-ring of the 6-6 SBU *(Fig. 5)*. What is really of interest is to get an idea how the MO picture develops, if more than one Cu^{+I} is added. Because within the EH-MO model the interaction between the Cu species is proportional to the overlap integrals, we first look at the distance dependence of the s–s, s–p_σ, p_σ–p_σ and p_π–p_π overlap integrals *(Fig. 10)*. At distances above approximately 4 Å, the s–s overlap becomes very small, while the p_σ–p_σ overlap is still considerable. For this reason, we expect larger Cu–Cu interaction distances in excited states of p_σ character than in the 4s* region and electronic energy transfer to be more efficient. In case of silver, all overlap integrals at 4 Å are large, and for p_σ–p_σ at 10 Å it is still not negligible. This means that the interaction radius of the Ag-atom is much larger than that of the Cu-atom which is probably the reason for some of the specific properties of Ag zeolites.
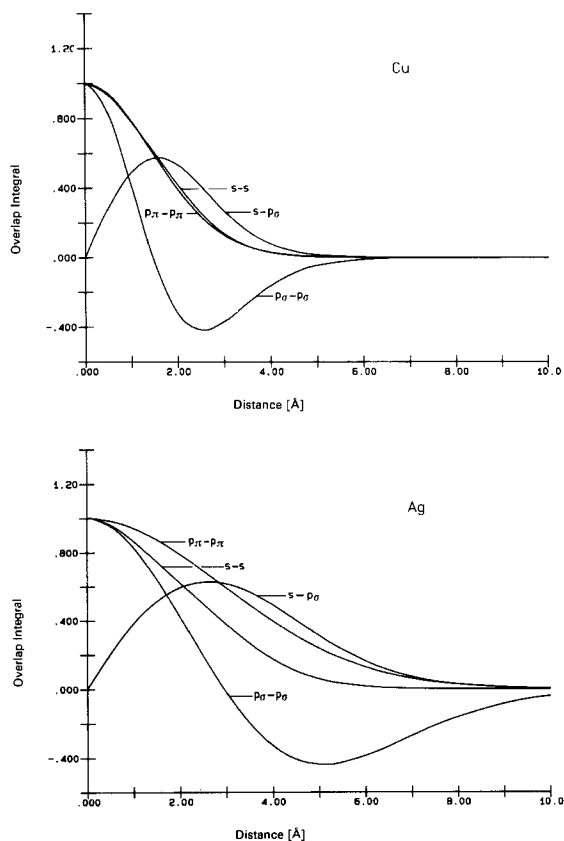

Fig. 10. *Overlap integrals between two Cu centers (top) and two Ag centers (bottom)*
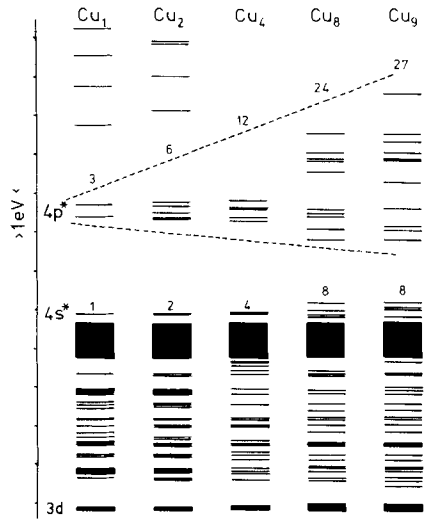
Fig. 11. *Electronic structure of 1, 2, 4, 8, and 9 Cu⁺¹ in a β-cage*. The number of 4s*-type and 4p*-type orbitals is indicated. The nearest neighbour Cu-O distances are in all cases 2.0 Å.

To derive the correlation diagram shown in *Fig. 11*, the Cu–Cu distances where chosen as follows: 6.92 Å in the Cu$_2$-β-cage, 4.0 Å in the tetrahedral Cu$_4$, the cubic Cu$_8$, and the Cu-atoms on the edges of the cubic body centered Cu$_9$. Although there is some 4s*–4p* mixing, a region of 4s*-type orbitals and another one of 4p*-type orbitals develop. But the size of the β-cage is too small to allow the formation of a band structure. The levels are distinctly quantized, but the interaction between the Cu-centers seem to be large enough in these geometrical arrangements that, if we add an electron into the 4s* region either by reduction or by an electronic or thermal 4s*←HOMO excitation, every Cu-atom will know about this electron. The same is true, if an electron is added to the 4p* region. In both cases, very efficient energy transfer is expected. It seems, that the situation of several Cu-centers in a β-cage has some similarities with the exciton states of semiconductor colloids [52] [53]. According to our results, synthesis of dehydrated Cu⁺¹ zeolites of any color should be accessible, depending on the copper concentration.

4. Electronic Structure of [Ag$_3$(H$_2$O)$_3$]³⁺ in a β-Cage. – In a previous paper, we have already described some properties of Ag⁺ and Ag⁰ in the 6-6 SBU. Copper and silver differ markedly in size. The Ag⁰ and Ag⁺ are much larger than Cu⁰ and Cu⁺¹. For this reason the antibonding interaction of the Ag 5s and 5p orbitals with the zeolite O orbitals is larger than in case of the Cu 4s, 4p orbitals [48]. The much larger interaction radius of Ag with respect to Cu is probably responsible for many specific properties encountered in Ag compounds.

It was found that Ag⁺ zeolite A that has been dehydrated at room temperature contains the [Ag$_3$(H$_2$O)$_3$]³⁺ species in the β-cage [54]. The H$_2$O molecules remain in this cluster up to temperatures of about 350°. As already mentioned, reversible color changes can be observed upon dehydration-hydration of Ag zeolites [9]. To understand the electronic structure of this hydrated Ag cluster, calculations have been carried out using the geometry with C_{3v} symmetry reported by *Kim* and *Seff* [54].
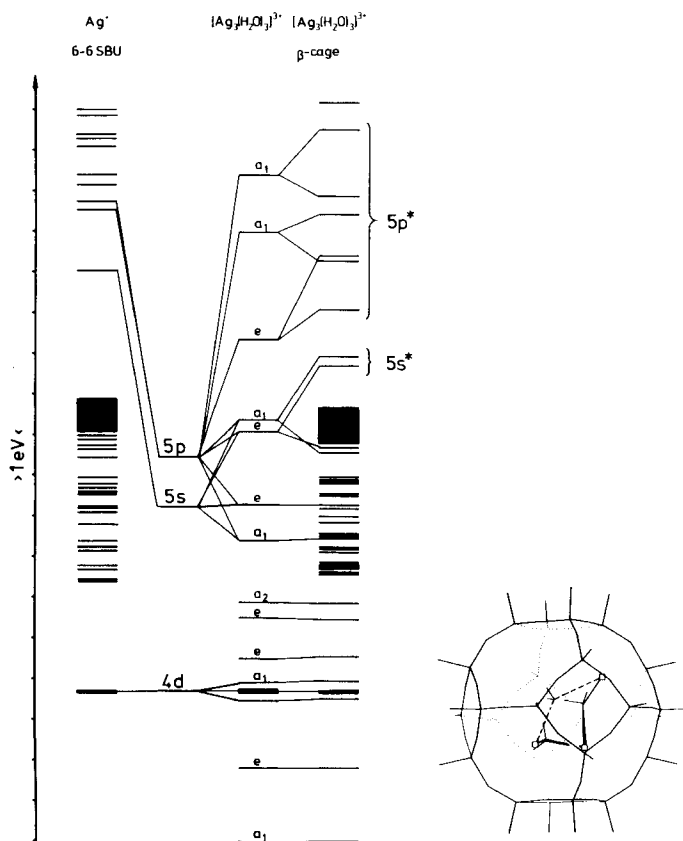
Fig. 12. *Comparison of the electronic structure of a Ag^{+1} in the 6-6 SBU, free [Ag$_3$(H$_2$O)$_3$]$^{3+}$, and this cluster in the* β-*cage.* The structure of [Ag$_3$(H$_2$O)$_3$]$^{3+}$ is indicated on the right side. The highest-occupied orbital of [Ag$_3$(H$_2$O)$_3$]$^{3+}$ is of a_2 symmetry and mainly localized on the H$_2$O O-orbitals.

The results of this calculation are reported in *Fig. 12,* where we compare the electronic structure of silver in the 6-6 SBU with that of [Ag$_3$(H$_2$O)$_3$]$^{3+}$ and {β-cage-[Ag$_3$(H$_2$O)$_3$]$^{3+}$}. First of all, it is interesting that the interaction of the [Ag$_3$(H$_2$O)$_3$]$^{3+}$ with the β-cage is strong. The lowest unoccupied orbitals, which are mainly localized on the Ag shift to significantly higher energy. As in the case of the Ag(6-6) SBU, orbitals localized on the Ag, formed by 5s and 5p atomic orbitals, are found in the gap between the HOMO and the LUMO of the zeolite. Again, the ligand-field picture breaks down as soon as the Ag interacts with the zeolite O-atom. The electronic absorption spectrum is predicted to be largely dominated by 5s*←HOMO transitions in the region of 1000 nm and by 5p*←HOMO transitions between 500 nm and 260 nm. We expect spontaneous 5s*←5p* emission to be an efficient process. The 5s* and 5p* states are largely delocalized, and significant s–p mixing is observed. Similar to the case of the Cu^{+1}, the color changes observed in Ag$^+$ zeolites upon dehydration are due to zeolite-to-silver charge-transfer transitions, which become possible by silver-to-zeolite-oxygen coordination and disappears in the fully hydrated Ag$^+$ ions. Despite of the large Ag–Ag distance of 4.82 Å, the overlap integrals are still large as seen from *Fig. 10*.

For this reason, the excited states of this complex are mainly delocalized Ag←zeolite-oxygen charge-transfer states. As soon as an electron is filled into the metal states, a change in the geometry is expected and many new electronic transitions may become possible.

5. Conclusions. – Many interesting observations have been made on zeolites, and only few of them are reasonably well understood. It is now clear, however, that the highest-occupied orbital region, which in case of the β-cage with two SBU's attached to it consists of 163 levels in an energy interval of 0.86 eV, has to be described as a region of narrow-lying localized states and not as a band structure. No sign of the formation of a conduction band is found in the LUMO region. The colors observed in dehydrated Cu^{+I} zeolites and in dehydrated Ag^{+I} zeolites can be understood as charge-transfer transitions from the HOMO concentrated on the zeolite O-atom to the metal cations. The luminescence observed in dehydrated Cu^{+I} zeolites is due to $4s^* \leftarrow 4p^*$ transitions. We expect the electronic structure and the chemical and physical properties of Cu and Ag zeolites to depend significantly on the metal concentration in the zeolite. The induction of the self-sensitization of photo-oxygen evolution in Ag zeolites [24] is caused by the oxygen-to-metal charge-transfer transitions. Even in hydrated Ag zeolites, there is a sufficient fraction of silver ions partly coordinated to zeolite O-atom, so that the concentration of states allowing oxygen-to-zeolite transitions at about 370 nm is high enough to permit the initial photo-oxygen evolution. The zeolite framework is oxidized in each charge-transfer transition, so that finally O_2 can evolve and protons are produced [23] [24]. Since the oxidation states of Si^{+IV} and Al^{+III} are not changed in aqueous dispersions and no other reductant is available, the O_2 originates from H_2O. We would like to emphasize that the ligand-field picture is not able to explain the electronic structure of dehydrated Cu^{+I} and Ag^{+I} zeolites. The thermodynamic and kinetic properties of finely dispersed silver and copper are very different from those of bulk metal. It is, therefore, important to study the chemical reactivity of photochemically reduced metal-loaded zeolites by applying theoretical and experimental methods.

REFERENCES

[1] G. Calzaferri, L. Forss, *Chem. Phys. Lett.* **1984**, *103*, 296.
[2] G. Calzaferri, L. Forss, *Helv. Chim. Acta* **1986**, *69*, 873.
[3] W. Meier, 'Zeolite Structures in Molecular Sieves', Soc. Chem. Ind., London, 1968; D. W. Breck, 'Zeolite Molecular Sieves', Wiley, London, 1974; R. M. Barrer, 'Zeolites and Clay Minerals as Sorbents and Molecular Sieves', Academic Press, New York, 1978.
[4] O. Zakliarieva A-Phencheva, H. Böse, H. Förster, W. Frede, M. Grodzicki, *J. Mol. Struct. (Theochem.)* **1985**, *122*, 101; W. J. Mortier, J. Sauer, J. A. Lercher, H. Noller, *J. Phys. Chem.* **1984**, *88*, 905; J. Sauer, R. Zahradnik, *Int. J. Quantum Chem.* **1984**, *XXVI*, 793; H. H. Dunken, R. Hoffmann, *Z. Phys. Chem. NF* **1981**, *125*, 207; S. Beran, P. Jirů, B. Wichterlová, *J. Phys. Chem.* **1981**, *85*, 1951; J. Sauer, P. Hobza, R. Zahradnik, *ibid.* **1980**, *84*, 3318; S. Berau, J. Dubsky, *Chem. Phys. Lett.* **1980**, *71*, 300.
[5] L. R. Gellens, W. J. Mortier, R. Lissilour, A. Le Beuze, *J. Phys. Chem.* **1982**, *86*, 2509; R. A. Schoonheydt, M. B. Hall, J. H. Lunsford, *Inorg. Chem.* **1983**, *22*, 3834.

[6] L. Riekert, *Ber. Bunsenges. Phys. Chem.* **1969**, *73*, 331.
[7] H. Beyer, P. A. Jacobs, J. B. Uytterhoeven, *J. Chem. Soc., Faraday Trans. 1* **1976**, *72*, 674.
[8] D. Hermerschmidt, R. Haul, *Ber. Bunsenges. Phys. Chem.* **1980**, *84*, 902.
[9] M. Ralek, P. Jiru, O. Grubner, H. Beyer, *Collect. Czech. Chem. Commun.* **1962**, *27*, 142.
[10] K. Narita, *J. Luminesc.* **1971**, *4*, 73.
[11] R. Kellerman, J. Texter, *J. Chem. Phys.* **1979**, *70*, 1562.
[12] P. A. Jacobs, J. B. Uytterhoeven, H. K. Beyer, *J. Chem. Soc., Faraday Trans. 1* **1979**, *75*, 56.
[13] J. Texter, Th. Gonsiorowski, R. Kellerman, *Phys. Rev. B* **1981**, *23*, 4407.
[14] L. R. Gellens, W. J. Mortier, J. B. Uytterhoeven, *Zeolites* **1981**, *1*, 11.
[15] G. A. Ozin, F. Hugues, *J. Phys. Chem.* **1983**, *87*, 94.
[16] D. R. Brown, L. Kevan, *J. Phys. Chem.* **1986**, *90*, 1129.
[17] J. R. Morton, K. F. Preston, *J. Magn. Reson.* **1986**, *68*, 121.
[18] J. Texter, R. Kellerman, Th. Gonsiorowski, *J. Phys. Chem.* **1986**, *90*, 2118.
[19] J. Texter, R. Kellerman, Th. Gonsiorowski, *J. Chem. Phys.* **1986**, *85*, 637.
[20] M. Narayana, L. Kevan, *J. Chem. Phys.* **1985**, *83*, 2556.
[21] P. A. Jacobs, J. B. Uytterhoeven, *J. Chem. Soc., Chem. Commun.* **1977**, 128.
[22] S. Leutwyler, E. Schumacher, *Chimia* **1977**, *31*, 475.
[23] B. Sulzberger, G. Calzaferri, *J. Photochem.* **1982**, *19*, 321.
[24] G. Calzaferri, S. Hug, Th. Hugentobler, B. Sulzberger, *J. Photochem.* **1984**, *26*, 109.
[25] G. Calzaferri, W. Spahni, *J. Photochem.* **1986**, *32*, 151.
[26] G. Calzaferri, W. Spahni, *Chimia* **1986**, *40*, 435.
[27] I. E. Maxwell, E. J. Drent, *J. Catal.* **1976**, *41*, 412.
[28] J. Texter, D. H. Strome, R. G. Herman, K. Klier, *J. Phys. Chem.* **1977**, *81*, 333.
[29] P. A. Jacobs, W. de Wilde, R. A. Schoonheydt, J. B. Uytterhoeven, H. Beyer, *J. Chem. Soc., Faraday Trans. 1* **1976**, *72*, 1221.
[30] D. H. Strome, K. Klier, *J. Phys. Chem.* **1980**, *84*, 981.
[31] D. H. Strome, K. Klier, *ACS Symposium Series* **1980**, 155.
[32] Y. Y. Huang, D. E. Mainwaring, *J. Chem. Soc., Chem. Commun.* **1974**, 584.
[33] Y. Y. Huang, *J. Am. Chem. Soc.* **1973**, *95*, 6636.
[34] T. Kubo, H. Tominaga, T. Kunugi, *Bull. Chem. Soc. Jpn.* **1973**, *46*, 3549.
[35] D. D. Davis, G. K. King, K. L. Stevenson, E. R. Birnbaum, J. H. Hageman, *J. Solid State Chem.* **1977**, *22*, 63.
[36] K. Sugasaka, A. Fujii, *Bull. Chem. Soc. Jpn.* **1976**, *49*, 82.
[37] G. R. Eulenberger, D. P. Shoemaker, J. G. Keil, *J. Phys. Chem.* **1967**, *71*, 1813. R. L. Gellens, J. V. Smith, J. J. Pluth, *J. Am. Chem. Soc.* **1983**, *105*, 51.
[38] G. D. Stucky, F. G. Dwyer, 'Intrazeolite Chemistry', ACS, Washington D.C., 1983.
[39] V. W. Day, W. G. Klemperer, V. V. Mainz, D. M. Millar, *J. Am. Chem. Soc.* **1985**, *107*, 8262.
[40] K. P. Huber, G. Herzberg, 'Constants of Diatomic Molecules', Van Nostrand Reinhold Company, New York, 1979.
[41] C. L. Frey, W. T. Collins, *J. Am. Chem. Soc.* **1970**, *92*, 5586.
[42] R. Hoffmann, *J. Chem. Phys.* **1963**, *39*, 1397.
[43] C. J. Ballhausen, H. B. Gray, 'Molecular Orbital Theory', Benjamin, New York, 1985; S. P. McGlynn, L. G. Vanquickenborne, M. K. Kinoshita, D. G. Carroll, 'Introduction to Applied Quantum Chemistry', Holt, Rinehart and Winston, New York, 1972.
[44] J. H. Ammeter, H. B. Bürgy, J. C. Thibeault, R. Hoffmann, *J. Am. Chem. Soc.* **1978**, *100*, 3686.
[45] H. Basch, A. Viste, H. B. Gray, *J. Chem. Phys.* **1966**, *44*, 10.
[46] V. I. Baranovskii, A. B. Nicol'skii, *Theor. Exp. Chem.* **1967**, *3*, 527.
[47] R. S. Mulliken, *J. Chem. Phys.* **1955**, *23*, 1833.
[48] G. Calzaferri, *Chimia* **1986**, *40*, 74.
[49] R. G. Herman, *Inorg. Chem.* **1979**, *18*, 995.
[50] T. Ichikawa, L. Kevan, *J. Phys. Chem.* **1983**, *87*, 4433.
[51] M. W. Anderson, L. Kevan, *J. Phys. Chem.* **1986**, *90*, 3206.
[52] A. Fojtik, H. Weller, U. Koch, A. Henglein, *Ber. Bunsenges. Phys. Chem.* **1984**, *88*, 969.
[53] L. Brus, *J. Phys. Chem.* **1986**, *90*, 2555.
[54] Y. Kim, K. Seff, *J. Phys. Chem.* **1978**, *82*, 921, 1071.
[55] G. Calzaferri, L. Forss, W. Spahni, *Chemie in Unsrer Zeit* **1987**, in press.